EFFECTS OF MID-TROPOSPHERIC DRY AIR ON EVOLUTION OF SUPERCELL STORMS

P10.145

Takumi Honda*, Tetsuya Kawano, and Ryuichi Kawamura
Kyushu University, Fukuoka, Japan

1. Introduction

Supercell storms are highly developing single convective clouds, which have a deep, persistent, rotating updraft. They are often accompanied by strong wind, heavy hailfalls, and extremely high lightning flash rates. Furthermore, the vast majority of strong to violent tornadoes (80%: Trapp et al. (2005b)) are associated with supercell storms. Although not all the developed supercell storms (mesocyclones) are followed by the tornadoes (Trapp et al. (2005a)), they produce a favorable condition for tornadogenesis by enhancing an upward perturbation pressure gradient force (Markowski et al. (2012)). Thus, understanding the conditions of the supercell development results in improvements of the tornadogenesis predictability.

Influences of the mid-tropospheric moisture on the storm evolution are not sufficiently examined because the relatively coarse observation is only available. Dry air aloft strongly affects the storm evolution through both the downdraft acceleration by enhanced evaporation of hydrometeors (Gilmore and Wicker (1998), hereafter GW98) and the updraft deceleration by the entrainment process (James and Markowski (2010), hereafter JM10).

An oft-cited previous study, GW98 examined the influence of mid-tropospheric dry air on the supercell storm evolution by using numerical experiments with several initial conditions. In the environment having dry air aloft, the low-level outflow is excessively enhanced, so that it cuts off the low-level warm-moist inflow, resulting in the storm weakening. However, they used a Kessler warm rain microphysics scheme, which had a bias of overestimation of evaporation rates (Gilmore et al. (2004)). Because storm behavior and evolution of cold pools strongly depend on the microphysics parametarization (e.g., Dawson et al. (2010)), the results of GW98 are somewhat questionable.

On the other hand, there is a more recent study, JM10, which performed numerical experiments similar to GW98 except that they used a modified Goddard microphysics scheme including ice processes (Braun and Tao (2000)). They suggested the cut-off mechanism proposed by GW98 does not occur and the entrainment process of dry air into ascending parcels mainly contributes to the storm weakening. However, they discussed mainly stationary squall lines having nearly two-dimensional structure. It is possible that there are some additional suppression processes in cases of the supercell having comprehensive three-dimensional structure.

In this study, we investigate the relationship between mid-tropospheric dry air and the supercell evolution using a non-hydrostatic numerical model with the cold rain microphysics scheme. It extends the works of GW98 and JM10 by the use of a cold rain microphysics scheme and detailed analyses of the supercell structure, respectively. We examined factors resulting in the differences of the storms by using the backward trajectory analysis.

2. Methodology

a. Numerical model

The Advanced Regional Prediction System (ARPS) Version 5.2.12 (Xue et al. (2000)), which solves a fully-compressible equation system is used in this study. The domain size is 100 km$\times$100 km horizontally and 20 km vertically. The horizontal grid interval is 500 m and the vertical grid size extends from 100 m at the ground to 700 m in the upper layer (52 levels). The lateral boundary conditions are open. The rigid walls are placed at the bottom and top boundaries with a Rayleigh damping layer above 14 km Above Ground Level (AGL). The 1.5-order turbulent kinetic energy closure scheme (Deardorff (1980)) is used for the parametarization of sub-grid scale turbulence. The WRF Single Moment 6 class scheme (WSM6; Hong and Lim (2006)), which predicts mixing ratios of water vapor, cloud water, rain, cloud ice, snow and hail, is applied to the microphysics parametarization scheme. The coriolis effects, topography, the curvature of the earth, the surface

[1] *Corresponding author address:* Takumi Honda, Dept. of Earth and Planetary Sciences, Graduate School of Sciences, Kyushu Univ., 6-10-1 Hakozaki, Higashi, Fukuoka 812-8581, Japan; e-mail: honda@weather.geo.kyushu-u.ac.jp

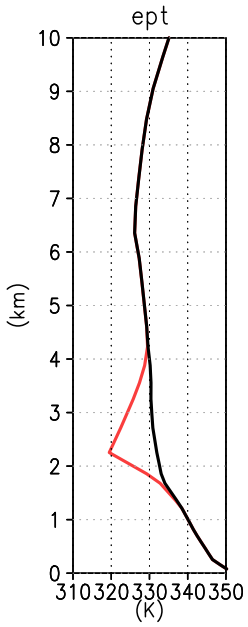

FIG. 1. Initial θ_e profiles for CNTL (black) and DRY40 (red).

friction and radiation processes are excluded to simplify analyses. The simulations are run for 5 hours with time steps of 3.0 s and 1.0 s for acoustic and the other modes, respectively.

b. Initial conditions

The composite sounding of Del City storm (Ray et al. (1981)), which produces the most typical supercell storm occurred on May 20 1977 at Oklahoma, is used as initial soundings of wind and temperature. An ellipsoidal thermal bubble having +2 K of maximum amplitude is placed at the 1.5 km AGL to initialize the convection. The diameters of bubble are horizontally 9 km and vertically 1.5 km, respectively.

To clarify the effects of dry air aloft, we modified a Relative Humidity (RH) sounding of the Del City storm below 5 km AGL (except near the surface) to 85%. This RH sounding is referred to as CNTL hereafter. As the initial RH soundings of the sensitivity experiments, we also made a dry sounding, having the dry layer spanning from 1.7 km AGL to 4.2 km AGL. The height of the dry-layer center is located at the 2.2 km AGL and the RH was reduced to 40% on the center (DRY40 sounding). The dry layer is equivalent to the low equivalent potential temperature (θ_e) layer. The initial θ_e profiles are shown in Fig. 1. CAPEs calculated by using virtual temperature profiles of each experiment are 2669 J kg^{-1}(CNTL) and 2700 J kg^{-1} (DRY40), respectively. The Mixed-Layer Lifting Condensation Level (MLLCL) is 710 m (890 mb) and the melting level ($0\ ^\circ$C) is located at the 3.8 km AGL. The bulk Richardson number is about 29.

3. Results

a. Behavior of simulated storms

Figure 2 shows evolutions of simulated storm structures in each experiment. At 60 min, structures and intensities of updrafts were similar (Figs. 2a, d, g, j). Downdraft regions of CNTL were smaller and weaker than those of DRY40 (Figs. 2a, d, g, j).

After 120 min, the storms began to decay in the DRY40 experiment (Figs. 2e, h). The updraft maximum, precipitation and following downdraft of DRY40 were significantly weakened. That of CNTL maintained the structure and intensity of storm convection until 180 min (Figs 2c, l).

Thermodynamic structures near the surface show that extremely low-θ_e air advects to the forward-flank region of the storms in DRY40 and DRY10 at 60 min (Figs. 3d, g). There was also a downdraft region corresponding to the Forward-Flank Downdraft (FFD). In contrast, the downdrafts corresponding to the FFD in CNTL and DRY40U were not significant and θ_e was relatively high at the surface.

After 120 min, the low-θ_e air flowed into the updraft from the forward-flank region of the storms in the DRY40 experiment (Figs. 3e, h). On the other hand, the updraft core regions were located along the gust front in the CNTL experiment, so that the low-θ_e air did not flow into the updraft.

b. DRY40 storm weakening

When the DRY40 storm began to decay, buoyancy of the ascending parcels at the upper-level (5 km AGL) in DRY40 was weaker than that in CTL (not shown). Thus, the storm weakening in DRY40 results from the insufficient buoyancy acceleration in the updraft core region. In

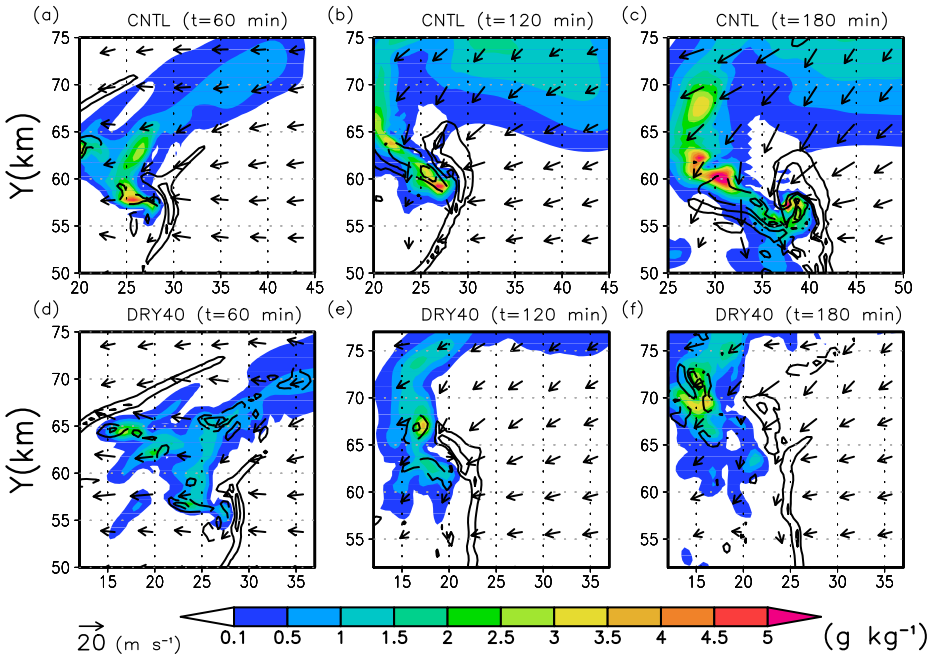

FIG. 2. Horizontal cross sections of rain mixing ratio (qr; shade), vertical velocity (w; contour), and horizontal wind (vector) in (a-c) CNTL, and (d-f) DRY40 at 1 km AGL.

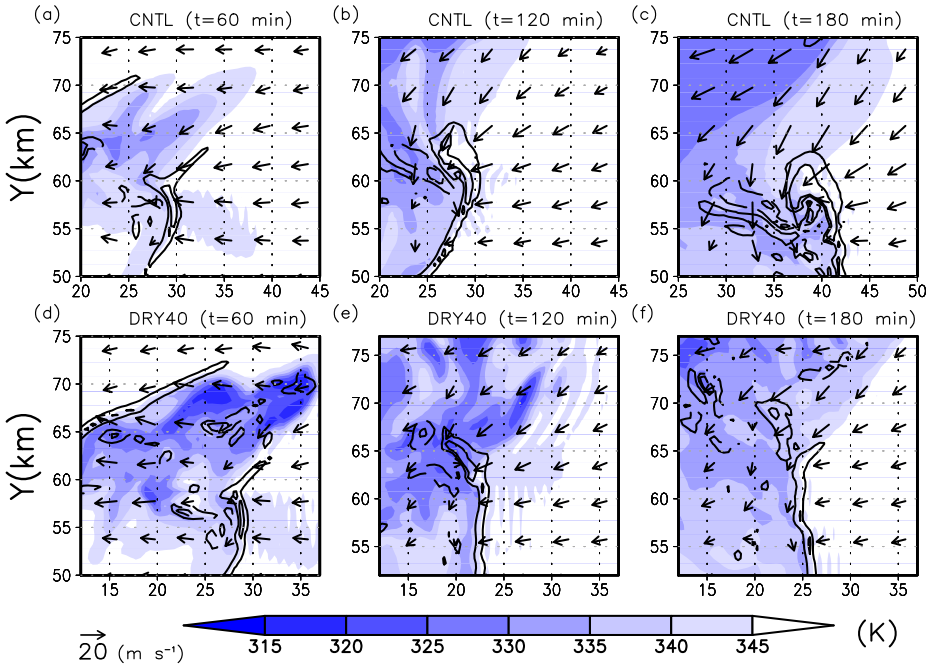

FIG. 3. As in Fig. 2, but for θ_e (shade) at 0.35 km AGL.

order to clarify the causes of the buoyancy difference, we calculated backward trajectories from the upper-level (5 km AGL) updraft core regions at 130 min. The three-dimensional wind field linearly interpolated from model outputs (1 min time intervals) was used to trajectory calculations with a fourth-order Runge-Kutta method.

In both CNTL and DRY40, most parcels originated from below 1 km AGL. Figure 4 shows averaged trajectory paths and θ_e evolutions in each experiment. Before ascending (120 min), the parcels existed at 800 m AGL (DRY40) and 500 m AGL (CNTL), respectively (Fig. 4a). The origin height and θ_e (DRY40: 343 K, CNTL: 345 K) of the trajectories were consistent with initial θ_e soundings (Figs. 1b, 4b). In DRY40, parcels existed around 500 m AGL at 120 min could not ascend to 5 km AGL since θ_e of the air was too low (Fig. 3e), so that the Level of Free Convection (LFC) of the air was located at the relatively higher altitude. Thus, the less buoyancy in DRY40 partly caused by the relatively-higher ascending-parcel origin height, reflecting the low-θ_e air advection near the surface.

Not only the differences of θ_e and following LFC before ascending but also the entrainment process played an important role in suppressing the convection in DRY40. The θ_e evolution along the trajectory in the DRY40 experiment showed a rapid decrease after 128 min (Fig. 4). In the dry layer (1.7 km- 4.2 km AGL), environmental θ_e was smaller than that of the ascending parcel (Figs. 1b, 4b). Thus, the rapid θ_e decreasing of the ascending parcel in DRY40 reflected the significant entrainment process of the environmental low-θ_e air. In contrast, the θ_e evolution in CNTL did not decrease significantly with time. This fact was caused by the presence of relatively high-θ_e air around the mid-troposphere and relatively low entrainment rate , reflecting the rapid upward motion of the parcels (Fig. 4a).

Figure 4b showed that the θ_e evolution in CNTL rapidly increased with time after 129 min. Then, the height of the parcel was 4 km AGL, corresponding to the melting level (Fig. 1), so that the increase of θ_e resulted from diabatic heating following melting processes (see Arakawa (2004)). In fact, mixing ratios of ice particles along the trajectory in CNTL also increased, however, that in DRY40 did not increase, reflecting the relatively few amounts of hydrometeors (Fig. 4c).

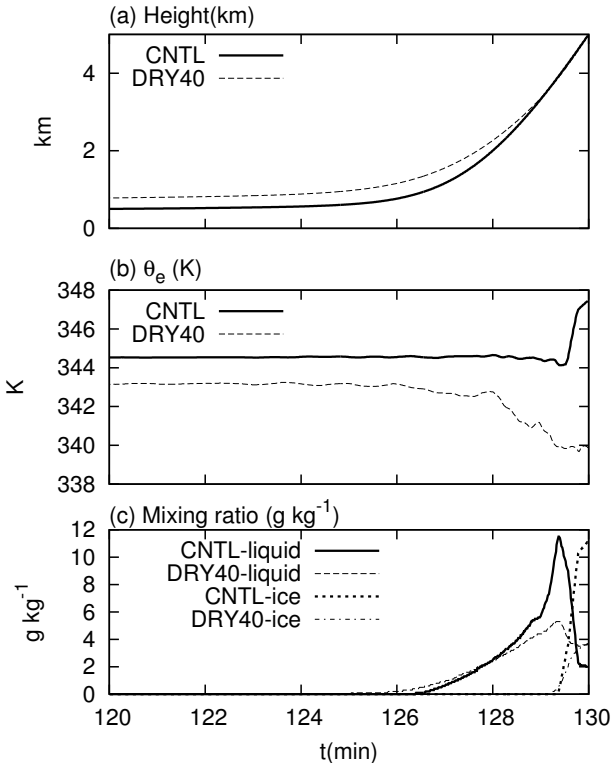

FIG. 4. Temporal variations in averaged (a) height, (b) θ_e, and (c) mixing ratios along trajectories of CNTL and DRY40 calculated from the upper-level updraft core region at 130 min (5 km AGL).

4. Discussion

As shown in above section, dry air aloft reduced the intensity and longevity of the supercell storm. Detailed analyses showed that the decay of the storm in the DRY40 experiment resulted from the following two processes. The one is the entrainment of dry air into the updraft, and another one is the low-θ_e air advection from mid-troposphere to the low-level updraft region, so that buoyancy of the ascending parcels reduced. The former process was similar to the mechanism indicated by JM10 but the later one was not suggested in JM10. Now, let us discuss this point.

A rate of the entrainment (ϵ) is represented as follows (Gregory (2001)):

$$\epsilon = C_\epsilon \frac{aB}{\overline{w}^{c2}}$$

where $\overline{w}^c$ is mean vertical velocity within the cloud area, B is buoyancy, and C_e(=0.25) and a(=1/6) are non-dimensional parameters. Thus, strong vertical velocity reduces the entrainment rate.

The latter process depends on the three-dimensional storm structure following the environmental wind (especially directional) shear. The storm downdrafts transporting the low-θ_e air are driven by the loading and latent cooling of the hydrometeors. Thus, the downdraft location and structure relate to the wind direction and following distributions of hydrometeors at each level. Squall lines analyzed by JM10 have nearly two-dimensional structure because they develop under unidirectional shear environment. The most hydrometeors produced by the convection flow into the rear side of the system, so that the downdrafts are located at the rear side of the convection. Thus, the low-θ_e air originated from mid-troposphere does not flow into the low-level updraft region in the squall lines analyzed by JM10.

JM10 also examined the case of the supercell storm with dry air aloft but did not suggest the low-θ_e air advection at the low level, resulting in the storm weakening. However, in fact, the low-θ_e advection process also acted in JM10. The entrainment process of dry air becomes significant only within the dry layer. The updraft mass flux calculated in the supercell case of JM10 significantly reduced above the bottom of the dry layer (2.5 km AGL), while it also decreased below the dry layer (see JM10; Fig. 21). The decrease of the updraft mass flux below the dry layer is responsible for the low-θ_e advection process as shown in the present study.

The supercell storms analyzed by the present study usually develop under the strong velocity and directional shear environment, so that the downdraft and following the low-θ_e air may exist in front of the storm. In fact, the low-θ_e air advection did not occur in GW98 because they used an unishear (no directional shear) wind profile. Since the downdraft location strongly depends on the vertical wind profile, similar sensitivity experiments with different hodograph shapes should be carried out in future studies.

5. Summary and conclusions

The three-dimensional ideal supercell simulations were performed with several initial moisture profiles to understand effects of mid-tropospheric dry air on the supercell storm evolution. In the CNTL experiment, a typical supercell was reproduced and it maintained for more than three hours. However, the storm decayed after 130 min in the DRY40 experiment. The budget analysis of the vertical momentum equation showed that the buoyancy term within the updraft region was weaker in DRY40 than that in CNTL at that time. This difference contributed to the storm decay in DRY40.

To clarify the cause of the buoyancy weakening in the DRY40 experiment, the backward trajectories were calculated from the upper-level updraft core region at 130 min. In the CNTL experiment, the most parcels originated from near the surface, while the most parcels originated from around 1 km AGL in DRY40 since the parcels around the surface which advected from the mid-tropospheric dry layer had the relatively low (high) θ_e (LFC altitude).

The θ_e variation along the trajectories in DRY40 tended to decrease with time, corresponding to the entrainment process of environmental dry air into the updraft. The entrainment process acted from the storm initialization. However, the storm decay in DRY40 was significant after the advection of the low-θ_e air to near the surface. Thus, the contribution of the entrainment process to the storm decay was relatively small.

Acknowledgments.

The first author was supported by the Kyushu University Fund.

REFERENCES

Arakawa, 2004: The cumulus parameterization problem: Past, present, and future. *J. Climate.*, **17**, 2493–2525.

Braun, S. A. and W.-K. Tao, 2000: Sensitivity of high-resolution simulations of hurricane bob (1991) to planetary boundary layer parameterizations. *Mon. Wea. Rev.*, **128**, 3941–3961.

Dawson, D. T., M. Xue, J. A. Milbrandt, and M. K. Yau, 2010: Comparison of evaporation and cold pool development between single-moment and multimoment bulk microphysics schemes in idealized simulations of tornadic thunderstorms. *Mon. Wea. Rev.*, **138**, 1152–1171.

Deardorff, J. W., 1980: Stratocumulus-capped mixed layer derived from a three-dimensional model. *Bound.-Layer Meteor.*, **18**, 495–527.

Gilmore, M. S., J. M. Straka, and E. N. Rasmussen, 2004: Precipitation and evolution sensitivity in simulated deep convective storms: Comparisons between liquid-only and simple ice and liquid phase microphysics. *Mon. Wea. Rev.*, **132**, 1897–1916.

Gilmore, M. S. and L. J. Wicker, 1998: The influence of midtropospheric dryness on supercell morphology and evolution. *Mon. Wea. Rev.*, **126**, 943–958.

Gregory, 2001: Estimation of entrainment rate in simple models of convective clouds. *Quart. J. Roy. Meteor. Soc.*, **127**, 53–72.

Hong, S.-Y. and J.-O. Lim, 2006: The wrf single-moment 6-class microphysics scheme (wsm6). *J. Korean Meteor. Soc.*, **42**, 129–151.

James, R. P. and P. M. Markowski, 2010: A numerical investigation of the effects of dry air aloft on deep convection. *Mon. Wea. Rev.*, **138**, 140–161.

Markowski, P., Y. P. Richardson, and Coauthors, 2012: The pretornadic phase of the goshen county, wyoming, supercell of 5 june 2009 intercepted by vortex2. part ii: intensification of low-level rotation. *Mon. Wea. Rev.*, **140**, 2916–2938.

Ray, P. S., B. C. Johnson, K. W. Johnson, J. S. Bradberry, J. J. Stephens, K. K. Wagner, R. B. Wilhelmson, and J. B. Klemp, 1981: The morphology of several tornadic storms on 20 may 1977. *J. Atmos. Sci.*, **38**, 1643–1663.

Trapp, R., G. Stumpf, and K. Manross, 2005a: A reassessment of the percent- age of tornadic mesocyclones. *Wea. Forecasting.*, **20**, 680–687.

Trapp, R., S. Tessendorf, E. S. Godfrey, and H. Brooks, 2005b: Tornadoes from squall lines and bow echoes. part i: climatological distribution. *Wea. Forecasting.*, **20**, 23–34.

Xue, M., K. K. Droegemeier, and V. Wong, 2000: The advanced regional prediction system (arps)a multiscale nonhydrostatic atmospheric simulation and prediction tool. part i: Model dynamics and verification. *Meteor. Atmos. Phys.*, **75**, 161–193.